Springer

KSME

Journal of Mechanical Science and Technology 27 (5) (2013) 1557~1568
www.springerlink.com/content/1738-494x
DOI 10.1007/s12206-013-0221-9

Numerical investigation of buoyancy effects on hydromagnetic unsteady flow through a porous channel with suction/injection †

Oluwole Daniel Makinde[1] and Tirivanhu Chinyoka[2,*]

[1]*Institute for Advanced Research in Mathematical Modeling and Computations, Cape Peninsula University of Technology, P. O. Box 1906, Bellville 7535, South Africa*
[2]*Center for Research in Computational and Applied Mechanics, University of Cape Town, Rondebosch 7701, South Africa*

(Manuscript Received March 23, 2012; Revised September 6, 2012; Accepted November 19, 2012)

Abstract

The paper focus on first and second laws analysis for flow and heat transfer inside a vertical channel made of two uniformly porous parallel plates with suction/injection under the combined action of buoyancy force, transverse magnetic field and constant pressure gradient. Both vertical walls are kept isothermal at the same temperatures and the flow of the conducting fluid is assumed to be unsteady with variable viscosity. The nonlinear governing equations in Cartesian coordinate are obtained and solved numerically using semi-implicit finite difference techniques to develop expressions for velocity and temperature profiles. The entropy generation number, irreversibility distribution ratio and Bejan number are presented graphically and discussed quantitatively for various values of the embedded parameters.

Keywords: Porous channel flow; Buoyancy force; Heat transfer; Entropy generation; Magnetic field

1. Introduction

Analysis of the flow of an electrically conducting fluid in a porous channel in the presence of a transverse magnetic field is of special technical significance because of its widespread engineering and industrial applications such as in geothermal reservoirs, nuclear reactor cooling, MHD marine propulsion, electronic packages, micro electronic devices, thermal insulation, and petroleum reservoirs. Some other quite promising applications are in the field of metallurgy such as MHD stirring of molten metal and magnetic-levitation casting. This type of problem also arises in electronic packages and microelectronic devices during their operation. The experimental investigation of modern MHD flow in a laboratory was first carried out by Hartmann and Lazarus [1]. Riley [2] studied buoyancy induced flow and transport in the presence of magnetic field. Chamkha [3] reported the unsteady natural convection in a porous channel in the presence of magnetic field. For rectangular vertical duct, Hunt [4] and Buhler [5] analyzed the fluid flow problem in magnetic field with or without buoyancy effect. For conducting fluid, Shercliff [6] analyzed the fluid flow characteristics in a pipe under transverse magnetic field. Alboussiere et al. [7] did an asymptotic analysis to study the buoyancy driven convection in a uniform magnetic field. Makinde and Aziz [8] reported the effects of magnetic field and convective heat transfer on mixed convection from a vertical plate embedded in a porous medium. The combined effects of variable viscosity and electrical conductivity on hydromagnetic flow and heat transfer between a fixed plate and moving parallel plate was numerically analyzed by Makinde and Onyejekwe [9]. All the above mentioned references are very much restricted to first law analysis in the thermodynamic point of view.

Meanwhile, the contemporary trend in the field of heat transfer and thermal design is the second law analysis and its design-related concept of entropy generation minimization. The foundation of knowledge of entropy production goes back to Clausius and Kelvin's studies on the irreversible aspects of the second law of thermodynamics. Since then the theories based on these foundations have rapidly developed. However, the entropy production resulting from combined effects of velocity and temperature gradients has remained untreated by classical thermodynamics, which motivates many researchers to conduct analyses of fundamental and applied engineering problems based on second law analysis. Entropy generation is associated with thermodynamic irreversibility, which is common in all types of heat transfer processes. Moreover, in thermodynamical analysis of flow and heat transfer processes, one thing of core interest is to improve the thermal systems to avoid the energy losses and fully utilize the energy resources. Since the pioneering work of Bejan [10, 11], many investiga-

*Corresponding author. Tel.: +27 021 650 3198, Fax.: +27 021 650 2334
E-mail address: chinyok@vt.edu
† Recommended by Associate Editor Yang Na

tions have been made on entropy generation analysis [12-17]. Sahin [18] investigated the second law analysis for a viscous fluid in a circular duct with isothermal boundary conditions. Tasnim and Mahmud [19] studied the first and second law characteristics of the flow and the heat transfer inside a vertical channel embedded in a porous medium under the influence of transverse magnetic field. Mahmud and Fraser [20] applied the second law analysis to heat and fluid flow due to forced convection inside a channel. The entropy generation in boundary layer flow was investigated by Arpaci and Selamet [21]. Makinde and Beg [22] studied the effect of magnetic field on entropy generation due to a reactive flow in a channel.

The purpose of this article is to analyze the first and second laws of thermodynamics with respect to inherent irreversibility in an unsteady flow of a viscous incompressible conducting fluid through a uniformly porous channel in the presence of suction/injection and a transversely imposed magnetic field with isothermal boundary condition. Expressions for dimensionless velocity, temperature and entropy generation number are presented graphically and discussed quantitatively.

The article is organized as follows: the mathematical model of the physical problem is described in section 2 leading to the relevant (dimensionless) governing equations. We follow this up in section 3 with the development of the mathematical tools to be used in analyzing the entropy generation and irreversibility. The numerical method of solution for the nonlinear set of governing partial differential equations is developed in section 4 and then employed in sections 5 and 6 to obtain and discuss the relevant graphical results. Concluding remarks follow in section 7.

2. Mathematical model

We consider unsteady flow of an incompressible electrically conducting viscous fluid through a vertical channel under the combined action of constant axial pressure gradient; buoyancy force and uniform suction/injection through channel walls in the presence of a transversely imposed magnetic field of strength B_0 (see Fig. 1). In addition, there is no applied electric field and all of the Hall effects are neglected. Since the magnetic Reynolds number is very small for most fluid used in industrial applications, we assume that the induced magnetic field is negligible. The fluid temperature dependent variable viscosity ($\bar{\mu}$) is expressed as

$$\bar{\mu} = \mu_0 e^{-\gamma(T-T_0)} \tag{1}$$

where μ_0 is the initial fluid dynamic viscosity at the temperature T_0.

Under these conditions the continuity, momentum and energy equations governing the problem in may be written as [7, 9, 18, 20]

$$\frac{\partial \bar{u}}{\partial \bar{x}} = 0 \tag{2}$$

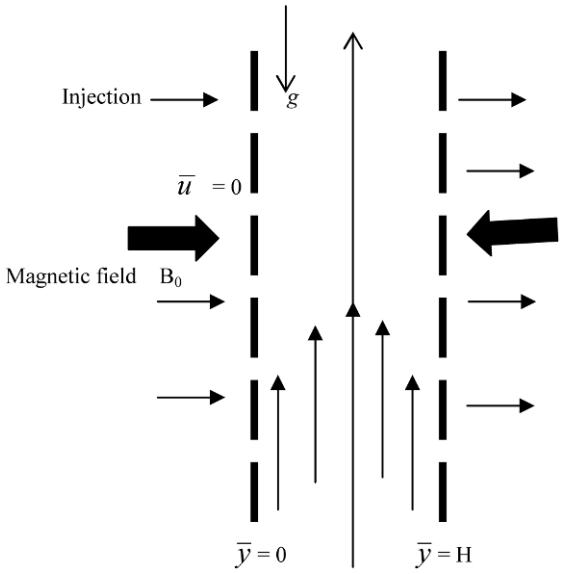

Fig. 1. Schematic diagram of the problem.

$$\frac{\partial \bar{u}}{\partial \tau} + V\frac{\partial \bar{u}}{\partial \bar{y}} = -\frac{1}{\rho}\frac{\partial \bar{p}}{\partial \bar{x}} + \frac{1}{\rho}\frac{\partial}{\partial \bar{y}}\left(\bar{\mu}\frac{\partial \bar{u}}{\partial \bar{y}}\right) - \frac{\sigma B_0^2 \bar{u}}{\rho} + g\alpha(T - T_0) \tag{3}$$

$$\frac{\partial T}{\partial \tau} + V\frac{\partial T}{\partial \bar{y}} = \frac{k}{\rho c_p}\frac{\partial^2 T}{\partial \bar{y}^2} + \frac{\bar{\mu}}{\rho c_p}\left(\frac{\partial \bar{u}}{\partial \bar{y}}\right)^2 + \frac{\sigma B_0^2 \bar{u}^2}{\rho c_p} \tag{4}$$

with the initial and boundary conditions given as

$$\bar{u}(0,\bar{y}) = 0,\ T(0,\bar{y}) = T_0 \tag{5}$$

$$\bar{u}(\tau,0) = 0,\ T(\tau,0) = T_w,\ \bar{u}(\tau,H) = 0,\ T(\tau,H) = T_w \tag{6}$$

where $(\bar{x},\bar{y})$ are the distance measured in the axial and normal directions respectively, τ is the time, ρ is the fluid density, k is the thermal conductivity, α is volumetric expansion coefficient, g is the gravitational acceleration, σ is the electrical conductivity, T is the fluid temperature, T_w is the channel wall's temperature, H is the channel width, T_0 is the fluid initial temperature, V is the uniform suction/injection velocity, $\bar{u}$ is the axial velocity, c_p is the specific heat at constant pressure and P is the fluid pressure. We introduce the following non-dimensional quantities into Eqs. (2)-(6):

$$y = \frac{\bar{y}}{H},\ x = \frac{\bar{x}}{H},\ u = \frac{\bar{u}}{V},\ v = \frac{\bar{v}}{V},\ \mu = \frac{\bar{\mu}}{\mu_0},\ \theta = \frac{T - T_0}{T_w - T_0},\ p = \frac{H\bar{p}}{\mu_0 V},$$
$$A = -\frac{\partial P}{\partial x},\ t = \frac{\tau V}{H},\ Br = \frac{\mu_0 V^2}{k(T_w - T_0)},\ \mathrm{Re} = \frac{\rho V H}{\mu_0},\ \beta = \gamma(T_w - T_0),$$
$$\mathrm{Pr} = \frac{\rho c_p H V}{k},\ M = \frac{\sigma B_0^2 H^2}{\mu_0},\ Gr = \frac{g\alpha(T_w - T_0)\rho H^2}{V\mu_0} \tag{7}$$

and obtain

$$\mathrm{Re}\left(\frac{\partial u}{\partial t}+\frac{\partial u}{\partial y}\right)=A+\frac{\partial}{\partial y}\left(e^{-\beta\theta}\frac{\partial u}{\partial y}\right)-Mu+Gr\theta \tag{8}$$

$$\mathrm{Pr}\left(\frac{\partial \theta}{\partial t}+\frac{\partial \theta}{\partial y}\right)=\frac{\partial^2\theta}{\partial y^2}+Bre^{-\beta\theta}\left(\frac{\partial u}{\partial y}\right)^2+BrMu^2 \tag{9}$$

with

$$u(0,y)=0,\ \theta(0,y)=0 \tag{10}$$

$$u(t,0)=0,\ \theta(t,0)=1,\ u(t,1)=0,\ \theta(t,1)=1 \tag{11}$$

where β is the viscosity variation parameter, Gr is the Grashof number, M is the magnetic field parameter, Br is the Brinkman number, Re is the suction/injection Reynolds number and Pr is the Prandtl number. Other quantities of interest in this study include the wall shear stress ι_w and the heat transfer rate at the channel surface q_w given as

$$\iota_w=\bar{\mu}\left.\frac{\partial \bar{u}}{\partial \bar{y}}\right|_{\bar{y}=0,\ H},\qquad q_w=-k\left.\frac{\partial T}{\partial \bar{y}}\right|_{\bar{y}=0,\ H} \tag{12}$$

and in dimensionless form, we obtain

$$C_f=\frac{\iota_w H}{\mu_0 V}=e^{-\beta\theta}\left.\frac{\partial u}{\partial y}\right|_{y=0,\ 1},\quad Nu=\frac{q_w H}{k(T_w-T_0)}=-\left.\frac{\partial \theta}{\partial y}\right|_{y=0,\ 1}. \tag{13}$$

3. Entropy analysis

Second law analysis in terms of entropy generation rate is a useful tool for predicting the performance of the engineering processes by investigating the irreversibility arising during the processes. According to Woods [23], the local entropy generation rate is defined as

$$S^m=\frac{\kappa}{T_w^2}\left(\frac{\partial T}{\partial \bar{y}}\right)+\frac{\bar{\mu}}{T_w}\left(\frac{\partial \bar{u}}{\partial \bar{y}}\right)^2+\frac{\sigma B_0^2}{T_w}\bar{u}^2. \tag{14}$$

The first term in Eq. (14) is the irreversibility due to heat transfer and the second term is the entropy generation due to viscous dissipation and third term is due to magnetic field. Using Eq. (7), we express the entropy generation number in dimensionless form as

$$Ns=\frac{H^2T_w^2S^m}{\kappa\left(T_w-T_0\right)^2}=\left(\frac{\partial \theta}{\partial y}\right)^2+\frac{Bre^{-\beta\theta}}{\Omega}\left(\frac{\partial u}{\partial y}\right)^2+\frac{MBr}{\Omega}u^2 \tag{15}$$

where $\Omega=(T_w-T_0)/T_0$ is the temperature difference parameter. In Eq. (15), the first term can be assigned as N_1 and the second term due to viscous dissipation as N_2, i.e.

$$N_1=\left(\frac{\partial \theta}{\partial y}\right)^2,\ N_2=\frac{Bre^{-\beta\theta}}{\Omega}\left(\frac{\partial u}{\partial y}\right)^2+\frac{MBr}{\Omega}u^2. \tag{16}$$

Following Bejan [10, 11], the irreversibility distribution ratio is defined as $\Phi = N_2 / N_1$. Heat transfer dominates for $0 \le \Phi < 1$ and fluid friction and magnetic field effects dominate when $\Phi > 1$. The contribution of both heat transfer and fluid friction with magnetic field effects to entropy generation are equal when $\Phi = 1$. Alternatively, the dominant effect of either heat transfer irreversibility or fluid friction with magnetic field irreversibility can be investigated using the Bejan number (Be) defined mathematically as

$$Be=\frac{N_1}{N_s}=\frac{1}{1+\Phi}. \tag{17}$$

Clearly, the Bejan number ranges from 0 to 1. $Be = 0$, is the limit where the fluid friction with magnetic field irreversibility dominates and Be = 1, corresponds to the limit where the heat transfer irreversibility dominates. The contribution of both heat transfer and fluid friction with magnetic field to entropy generation are equal when $Be = 1/2$.

In section 4, Eqs. (8)-(17) are solved numerically using a semi-implicit finite difference scheme.

4. Numerical procedure

Our numerical algorithm is based on the semi-implicit finite difference scheme and is implemented along the same lines as in, say, Refs. [24-27]. Implicit terms are taken at the intermediate time level $(N+\xi)$ where $0 \le \xi \le 1$. The discretization of the governing equations is based on a linear Cartesian mesh and uniform grid on which finite-differences are taken. We approximate both the second and first spatial derivatives with second-order central differences. The equations corresponding to the first and last grid points are modified to incorporate the boundary conditions. The semi-implicit scheme for the velocity component reads:

$$\begin{aligned}&\mathrm{Re}\frac{u_j^{(N+1)}-u_j^{(N)}}{\Delta t}+\mathrm{Re}\,u_y^{(N)}=A+\exp(-\beta\theta_j^{(N)})u_{yy}^{(N+\xi)}\\&+\exp(-\beta\theta_j^{(N)})\theta_y^{(N)}u_y^{(N)}-Mu^{(N+\xi)}+Gr\theta^{(N)}.\end{aligned} \tag{18}$$

In Eq. (18) it is understood that subscript y denotes partial differentiation under the finite difference framework described earlier, the subscript j represents the mesh position and the superscripts denote the time levels such that $\#^{(N+\xi)}=\xi\#^{(N+1)}+(1-\xi)\#^{(N)}$. Since the unsteady problem under investigation is posed as an initial value problem, given a solution at a time level (N), i.e. $\left[u^{(N)},\theta^{(N)}\right]$, the equations for the velocity solution at the subsequent time level $(N+1)$ reduce to:

$$\begin{aligned}&-r_1u_{j-1}^{(N+1)}+(\mathrm{Re}+M\Delta t\xi+2r_1)u_j^{(N+1)}-r_1u_{j+1}^{(N+1)}\\&=\exp licit\sim terms\end{aligned} \tag{19}$$

where the explicit terms contain terms prescribed at the earlier time level (N) and:

$$r_1 = \xi \frac{\Delta t}{\Delta y^2} \exp(-\beta \theta_j^{(N)}).$$

The solution procedure for $u^{(N+1)}$ thus reduces to inversion of tri-diagonal matrices which is an advantage over a full implicit scheme. The semi-implicit integration scheme for the energy equation is similar to that for the velocity:

$$\begin{aligned} &\Pr \frac{\theta_j^{(N+1)} - \theta_j^{(N)}}{\Delta t} + \Pr \theta_y^{(N)} = \theta_{yy}^{(N+\xi)} \\ &+ Br \exp(-\beta \theta_j^{(N)})[u_y^{(N)}]^2 + BrM[u^{(N)}]^2. \end{aligned} \tag{20}$$

The equation for $\theta^{(N+1)}$ thus becomes:

$$\begin{aligned} &-r\theta_{j-1}^{(N+1)} + (\Pr + 2r)\theta_j^{(N+1)} - r\theta_{j+1}^{(N+1)} \\ &= \exp licit \sim terms \end{aligned} \tag{21}$$

where $r = \xi \Delta t / \Delta y^2$. The solution procedure again reduces to inversion of tri-diagonal matrices. The schemes (19 & 21) were checked for consistency. For $\xi = 1$, these are first-order accurate in time but second order in space. The schemes in Ref. [24] have $\xi = 1/2$ which improves the accuracy in time to second order. We use $\xi = 1$ here so that we are free to choose larger time steps.

5. Results and discussion

Unless otherwise stated, we employ the parameter values:

$$\begin{aligned} &A = 1,\ \beta = 0.5,\ M = 0.5,\ Gr = 0.5,\ Br = 1,\ \Pr = 7.1, \\ &\mathrm{Re} = 1,\ \Delta y = 0.02,\ \Delta t = 0.5,\ t = 500. \end{aligned}$$

These will be the default values in this work and hence in any graph where any of these parameters is not explicitly mentioned, it will be understood that such parameters take on the default values.

5.1 Transient and steady flow profiles

We display the transient solutions in Figs. 2 and 3. Both figures show a transient increase in fluid quantities (velocity and temperature) until a steady state is reached.

5.2 Parameter dependence of solutions

In this section, we investigate the response of the velocity and temperature (at steady state) to varying values of the relevant parameters. To ensure that all solutions have indeed reached steady state, we employ a time of $t = 500$ in all graphs under this section. The response of the velocity and temperature to variations in the viscosity parameter (β) is illustrated in Figs. 4 and 5 respectively.

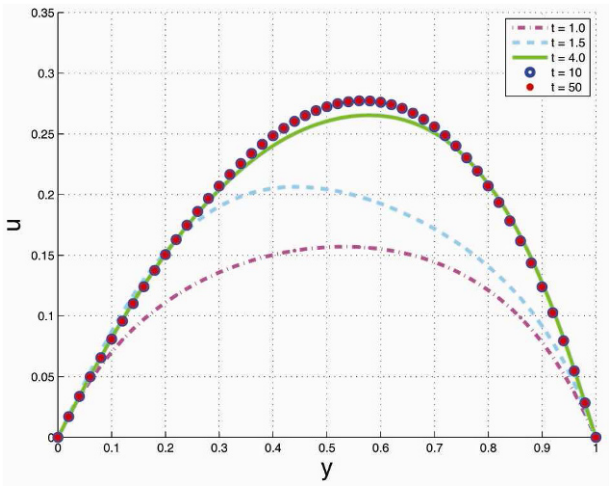

Fig. 2. Transient and steady state velocity profiles.

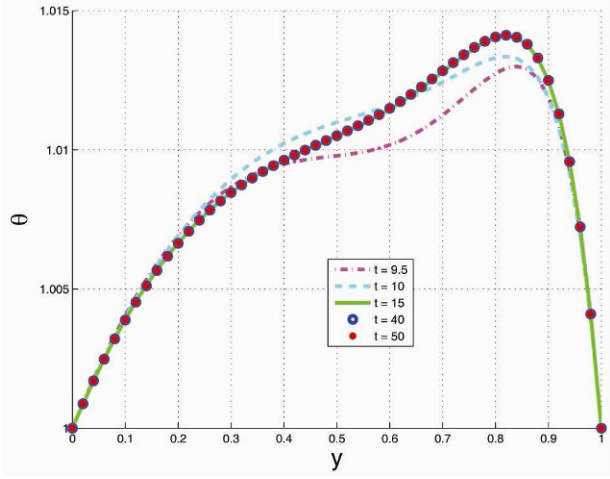

Fig. 3. Transient and steady state temperature profiles.

An increase in the viscosity parameter corresponds to a decrease in fluid viscosity and hence a reduced resistance to flow. This in turn leads to increased fluid velocity as shown in Fig. 4. The increased fluid velocity in turn increases the magnitude of the viscous heating sources terms in the energy equations and hence leads to increased fluid temperatures as illustrated in Fig. 5.

The response of the velocity and temperature to variations in the Brinkman number (Br) is illustrated in Figs. 6 and 7 respectively.

As previously explained, the increased strength of the viscous heating source terms (due to increases in the Brinkman number) is directly responsible for the increase in fluid temperature shown in Fig. 7. The temperature is strongly coupled to the velocity through the temperature dependent buoyancy terms and hence the recorded temperature increases (with increasing Br) lead to corresponding increases in the magnitude of the fluid velocity as shown in Fig. 6.

The suction Reynolds number primarily represents the strength of the suction/injection through the walls. Thus,

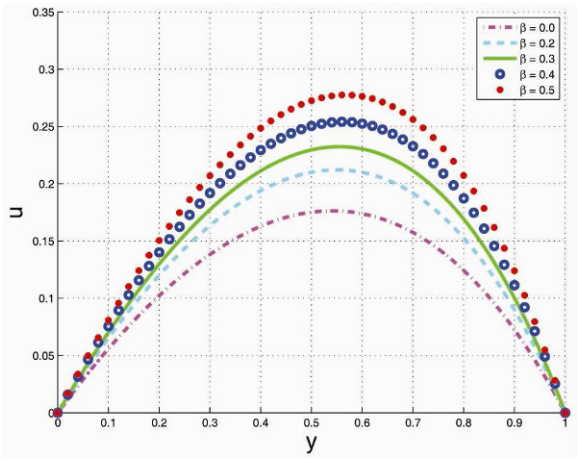

Fig. 4. Effects of viscosity parameter on steady state velocity.

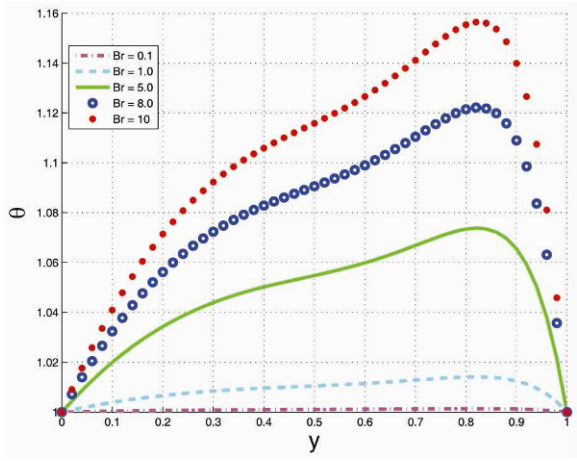

Fig. 7. Effects of Brinkman number on steady state temperature.

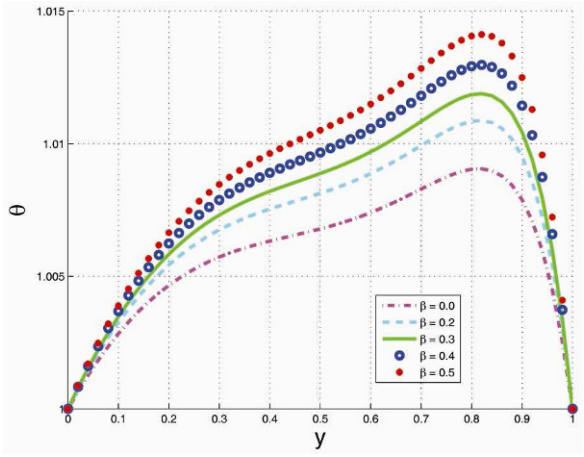

Fig. 5. Effects of viscosity parameter on steady state temperature.

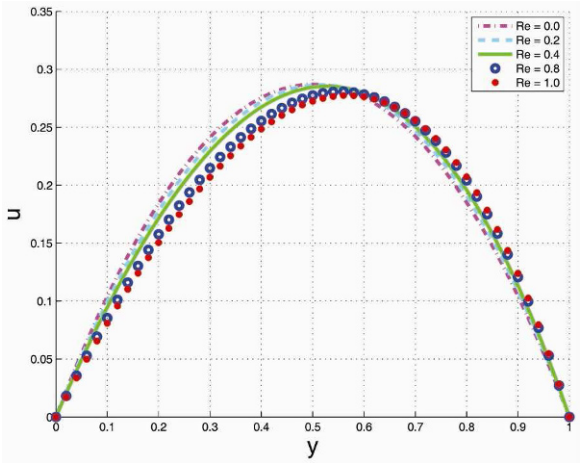

Fig. 8. Effects of the suction Reynolds number on steady state velocity.

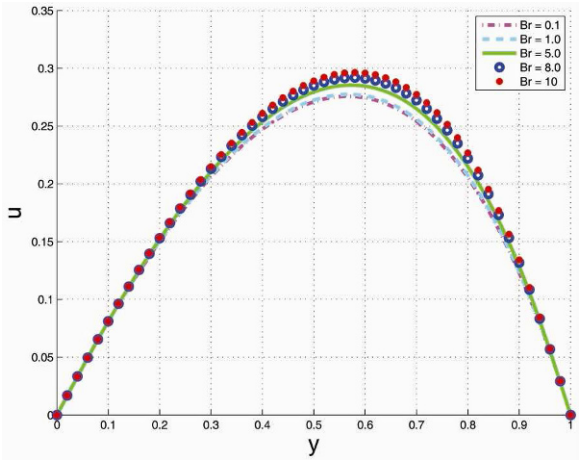

Fig. 6. Effects of Brinkman number on steady state velocity.

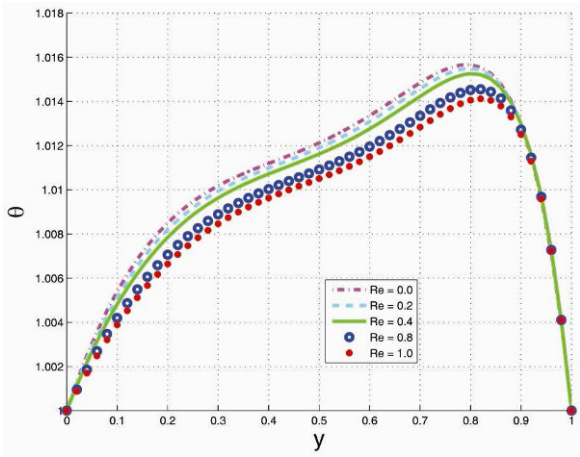

Fig. 9. Effects of the suction Reynolds number on steady state temperature.

$\mathrm{Re} = 0$ represents the case of (steady) plane Poiseuille flow in a channel with impermeable walls and $\mathrm{Re} > 0$ represents flow with constant suction/injection towards the right hand side direction. Figs. 8 and 9 respectively show the response of the fluid velocity and temperature to variations in the suction Reynolds number. We notice that as the suction Reynolds number moves away from zero, the region of maximum fluid velocity correspondingly moves away from the channel cen-

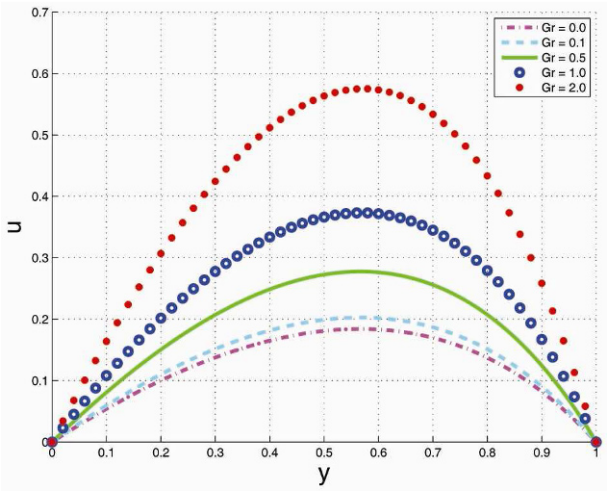

Fig. 10. Effects of Grashof number on steady state velocity.

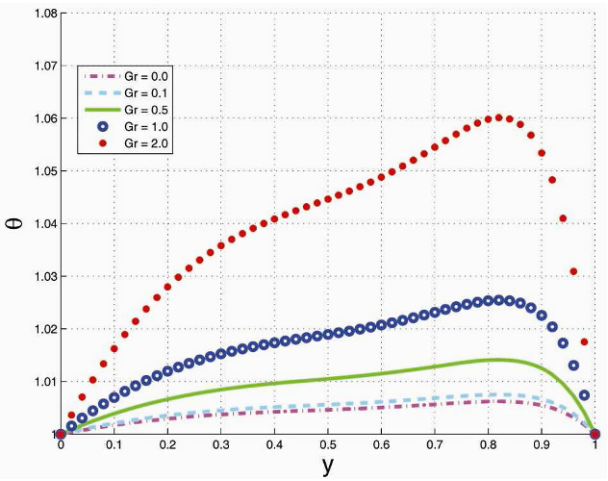

Fig. 11. Effects of Grashof number on steady state temperature.

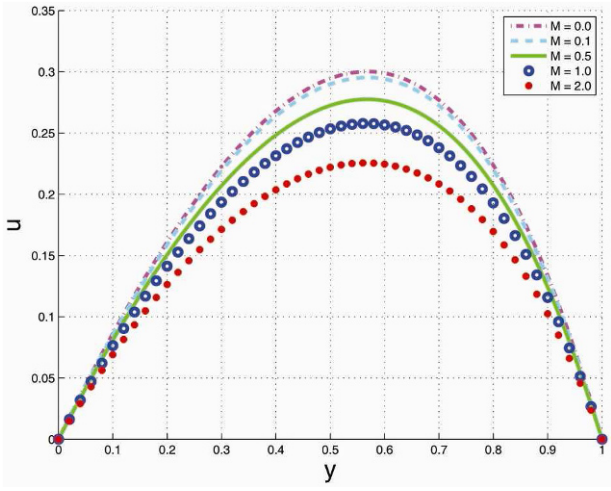

Fig. 12. Effects of the magnetic field strength on steady state velocity.

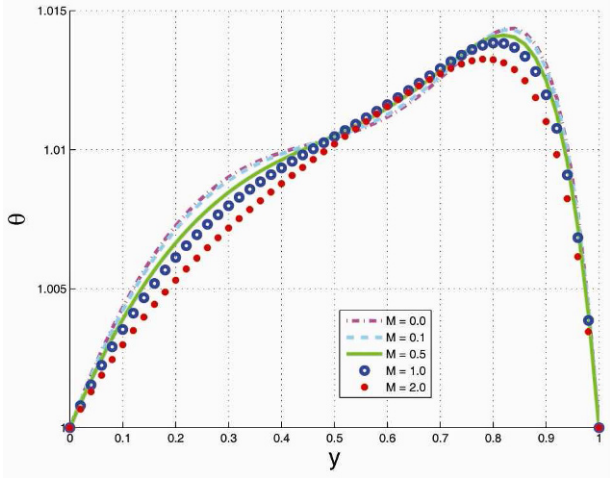

Fig. 13. Effects of the magnetic field strength on steady state temperature.

terline towards the direction in which the bulk fluid is "pushed" by the suction/injection cross flow. The presence of the cross flow is used to explain the reduction of the strength of the longitudinal velocity component u. In particular, the larger the strength of the cross flow (i.e. the higher the value of Re) the lower the magnitude of the longitudinal velocity component $u(y)$ as shown in Fig. 8. As explained before, the nature of the coupling of the velocity to the source terms in the energy equation leads to a corresponding reduction in fluid temperature with increased suction Reynolds numbers (i.e. with decreased longitudinal fluid velocity strength) as shown in Fig. 9.

The increase in the magnitude of the velocity with increasing Grashof number as illustrated in Fig. 10 is a consequence of the increased buoyancy source terms due to the higher values of Gr. The increased velocity in turn leads to increased fluid temperature due to the increased source terms, see Fig. 11. An increased magnetic field strength expectedly leads to decreased magnitudes in fluid velocity due to the increased resistance to flow, see Fig. 12. The magnitude of the temperature field however depends on a combination of the strength of the magnetic field M as well as the magnitude of the velocity field, both of which contributes to the energy sources, see Fig. 13.

5.3 Skin friction

The wall shear stress (at the right hand side wall, $y=1$) dependence on β is illustrated in Fig. 14 for varying values of the Brinkman number Br. Similarly, the wall shear stress dependence on Re is illustrated in Fig. 15 at different times and the wall shear stress dependence on M is illustrated in Fig. 16 for varying values of the Grashof number.

The results of Figs. 14-16 are consistent with the conclusions of the previous section, on parameter dependence of solutions. In general, parameters that decrease (increase) the fluid velocity correspondingly decrease (increase) the wall shear stress, respectively. This is so since (i) fluid viscosity at

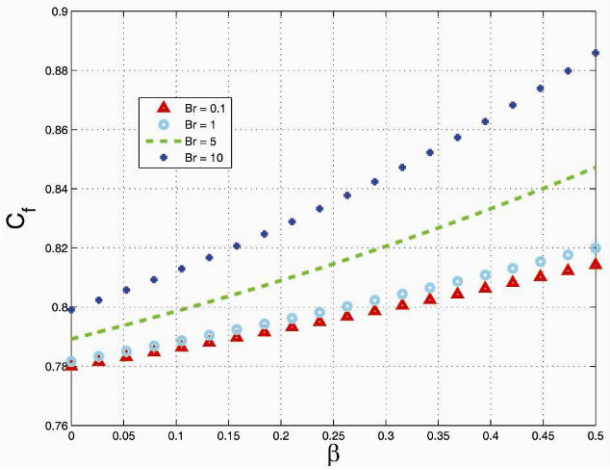

Fig. 14. Variation of wall shear stress with β and Br .

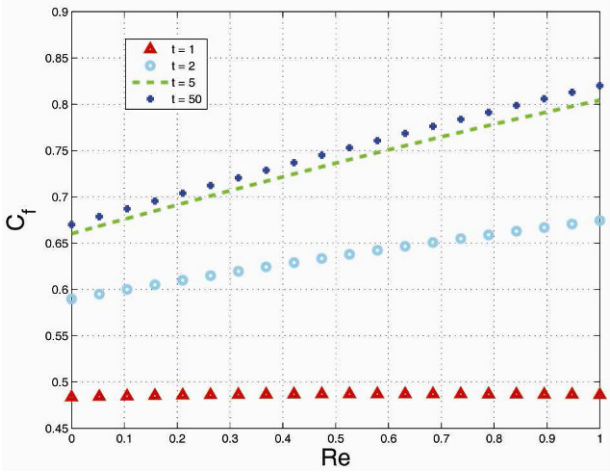

Fig. 15. Variation of wall shear stress with Re and t .

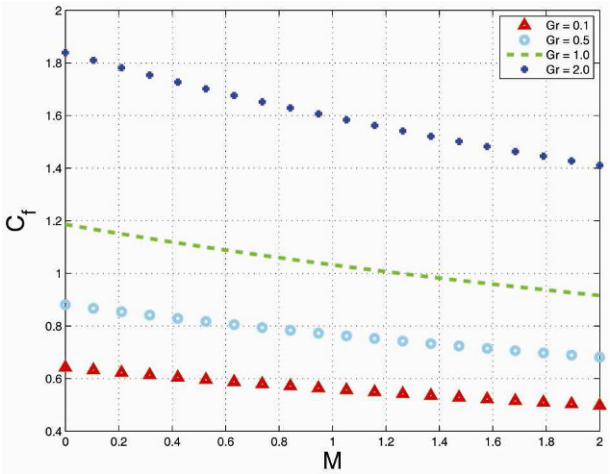

Fig. 16. Variation of wall shear stress with M and Gr .

the wall(s) remains constant due to the fixed wall temperatures while (ii) the decrease (increase) of the bulk flow velocity correspondingly decreases (respectively increases) velocity

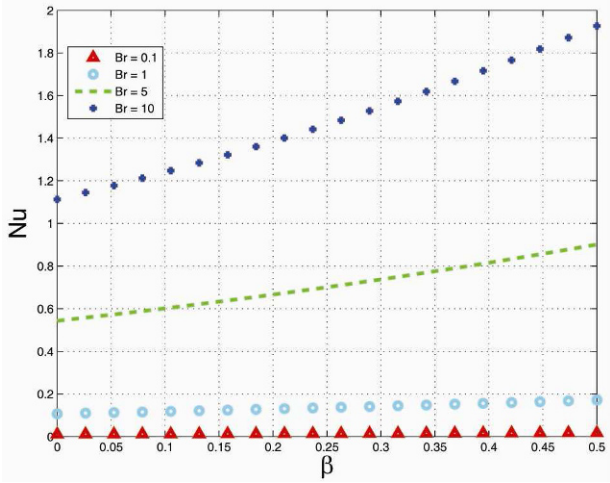

Fig. 17. Variation of wall heat transfer rate with β and Br .

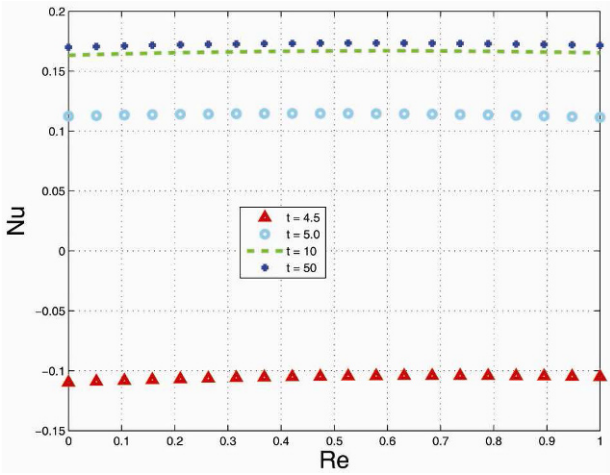

Fig. 18. Variation of wall heat transfer rate with Re and t .

gradients at the wall(s).

5.4 Wall heat transfer

The wall heat transfer rate (at the right hand side wall, $y = 1$) dependence on β is illustrated in Fig. 17 for varying values of the Brinkman number Br . Similarly, the wall heat transfer rate dependence on Re is illustrated in Fig. 18 at different times and the wall heat transfer rate dependence on M is illustrated in Fig. 19 for varying values of the Grashof number.

As with the wall shear stress, parameters that decrease (increase) the fluid temperature correspondingly decrease (increase) the wall heat transfer rate respectively.

5.5 Entropy generation

In this section, we plot the entropy generation rate Ns across the channel under varying parameter conditions.

Figs. 20-22 show the expected increase in Ns with corre-

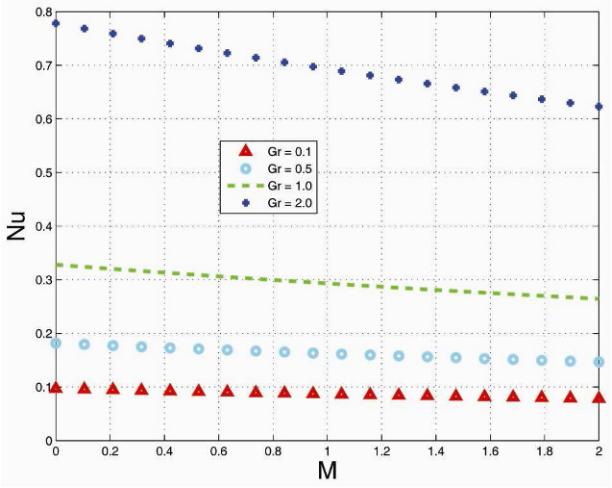

Fig. 19. Variation of wall heat transfer rate with M and Gr.

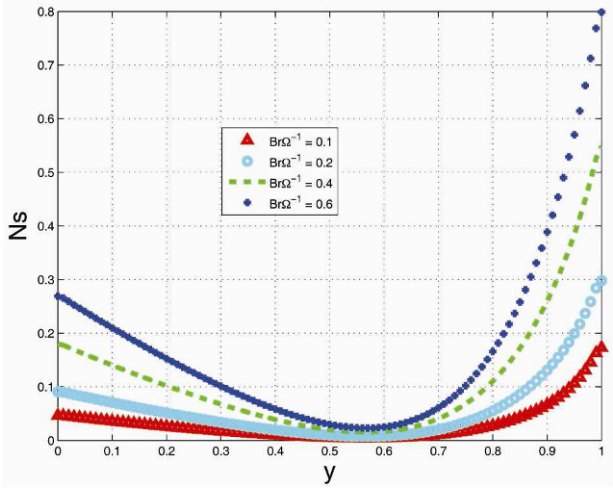

Fig. 20. Variation of entropy generation rate with y and $Br\Omega^{-1}$.

sponding increases in $Br\Omega^{-1}$, β and Gr respectively. This follows from the realization that increases in these parameters correspondingly increase the fluid friction with magnetic field contribution to the entropy generation. In Figs. 20 - 22, the entropy generation rate is expectedly maximum at the walls where velocity and temperature gradients as well as fluid viscosity are highest and minimum somewhere inside the channel in the proximity of the regions of maximum temperature and velocity and hence also minimum temperature and velocity gradients.

As the suction Reynolds number (Re) increases, the displacement of the velocity profiles towards the right means that the magnitudes of the velocity (and temperature) gradients decrease at the left wall but increase at the right wall. This explains (i) the opposite behavior in Ns shown in Fig. 23 at the opposite walls and (ii) why higher Ns values obtain at the right wall. Roughly similar behavior is observed with respect to the magnetic field, see Fig. 24. In this case the unequal effects at the opposite walls due to suction/injection result in the similar but unequal behavior in Ns at the opposite walls.

The time dependent behavior of Ns shown in Fig. 25 is almost similar to that illustrated in Figs. 20-22. Maximum entropy generation rate is recorded at the walls at all times and minimum values occur somewhere inside the channel in the proximity of the regions of maximum temperature and velocity.

5.6 Bejan number

In this section, we plot the Bejan number Be across the channel under varying parameter conditions. The analysis in this section is similar to that for the previous section with Ns now replaced by Be.

Fig. 26, shows as expected that higher values of $Br\Omega^{-1}$, which increase the magnitude of fluid friction with magnetic field irreversibility N_2 but has no effect on the heat transfer irreversibility N_1, increases the values of Φ leading to

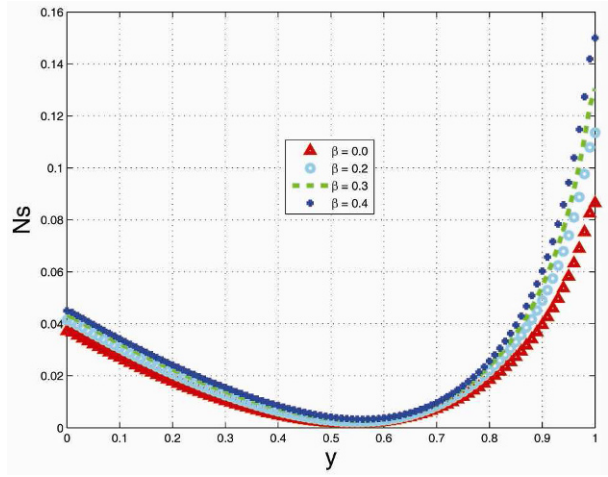

Fig. 21. Variation of entropy generation rate with y and β.

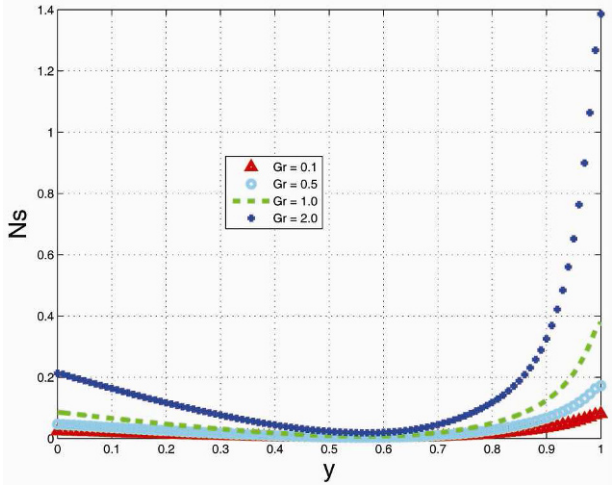

Fig. 22. Variation of entropy generation rate with y and Gr.

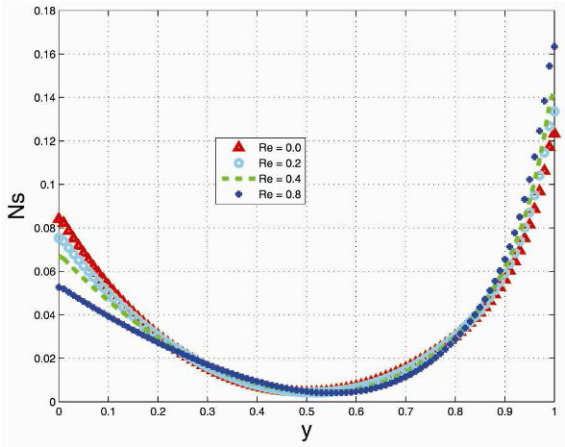

Fig. 23. Variation of entropy generation rate with y and Re .

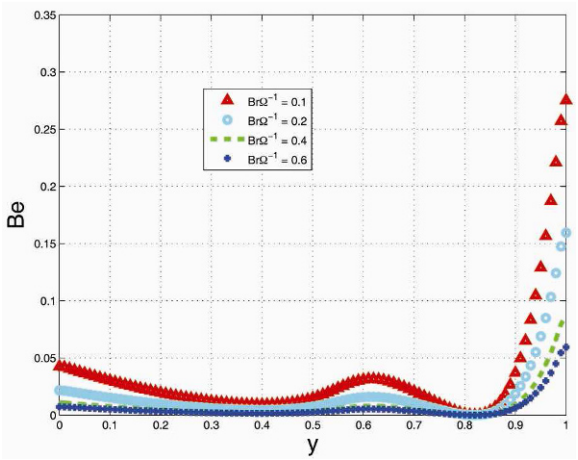

Fig. 26. Variation of Bejan number with y and $Br\Omega^{-1}$.

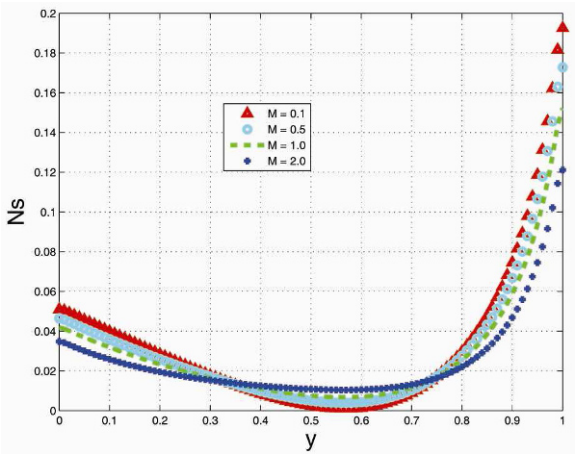

Fig. 24. Variation of entropy generation rate with y and M .

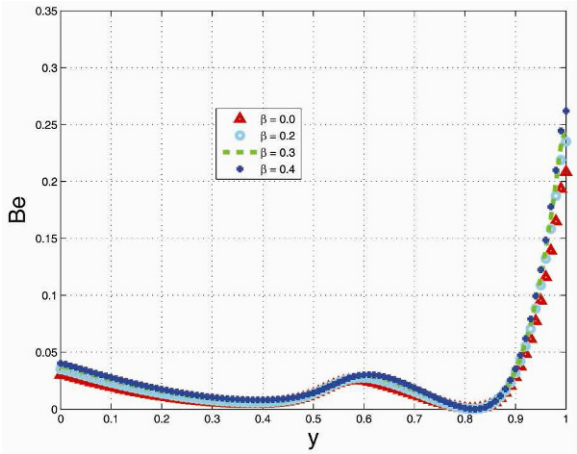

Fig. 27. Variation of Bejan number with y and β .

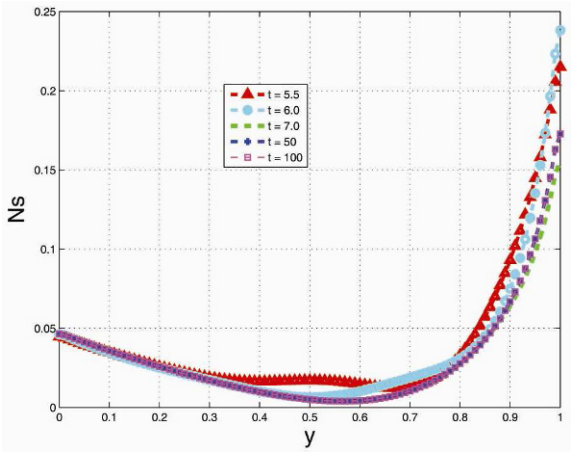

Fig. 25. Variation of entropy generation rate with y and t .

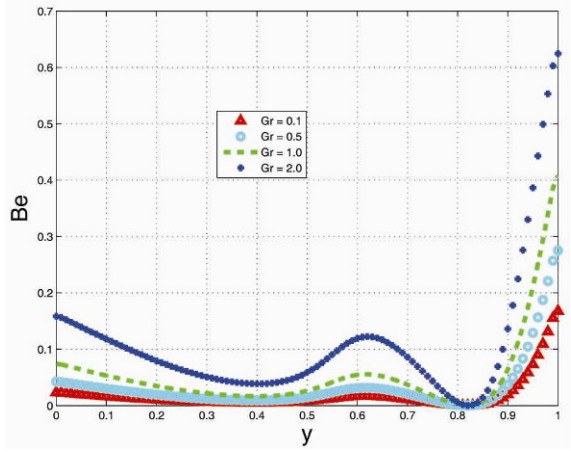

Fig. 28. Variation of Bejan number with y and Gr .

lower Bejan numbers.

The effects of β and Gr show their competing influence on N_1 and N_2. In general we notice that these parameters have a higher effect on the heat transfer irreversibility (N_1) than on fluid friction with magnetic field irreversibility (N_2) and hence an increase in either β or Gr gives correspondingly higher Bejan numbers as shown in Figs. 27 and 28.

Fig. 29 shows that as the Reynolds number increases (i) heat transfer irreversibility dominates over fluid friction with magnetic field irreversibility close to the walls as shown by

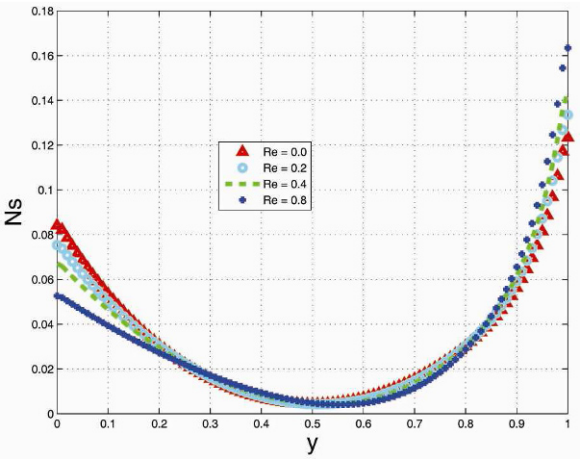

Fig. 29. Variation of Bejan number with y and Re .

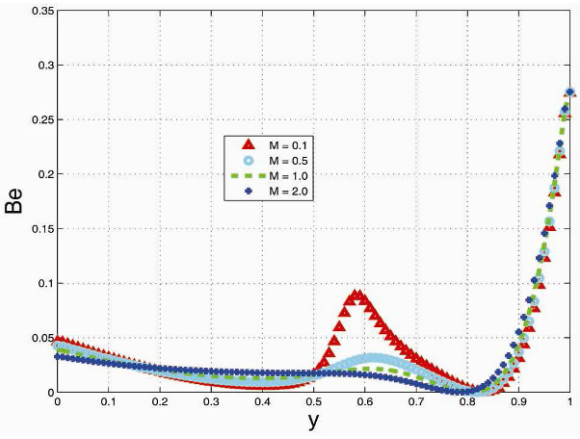

Fig. 30. Variation of Bejan number with y and M .

the decrease in the Bejan number in these regions, (ii) similar behavior is observed inside the channel just to the left the region of maximum velocity, but (iii) opposite behavior obtains just to the right the region of maximum velocity in which the Bejan number increases with Re .

Fig. 30 shows that as the magnetic field intensity increases (i) fluid friction with magnetic field irreversibility dominates over heat transfer irreversibility close to the right wall as shown by the increase in the Bejan number in this region, (ii) similar behavior is observed inside the channel just to the left the region of maximum velocity, but (iii) opposite behavior obtains just to the right the region of maximum velocity in which the Bejan number decreases with increasing SMS.

The time dependent behavior is illustrated in Fig. 31. Close to the walls, an interplay between both fluid friction with magnetic field and heat transfer irreversibility leads to positive values of the Bejan number ($0 < Be < 1$) in this wall region. Close to the left wall, the fluid friction with magnetic field irreversibility strongly dominates over heat transfer irreversibility. Close to the right wall, the strength of the fluid parameters will determine which mode of irreversibility dominates over the other. At our current parameters (with $Be < 0.5$) the

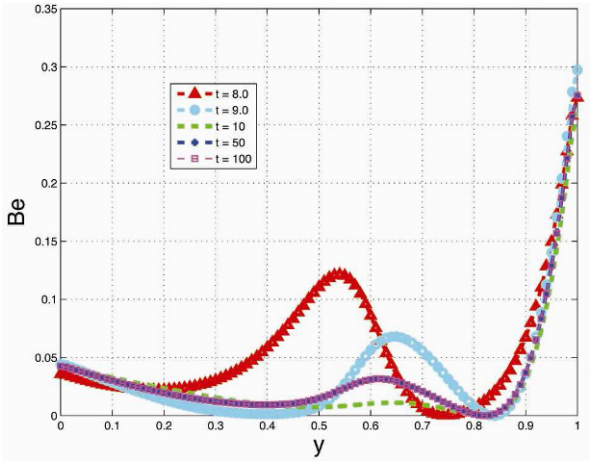

Fig. 31. Variation of Bejan number with y and t .

fluid friction with magnetic field irreversibility dominates over heat transfer irreversiility at this wall.

6. Entropy generation minimization

The minimization of the calculated entropy generation rate is of crucial importance in irreversibility analysis, we refer to Ref. [28] for a more comprehensive and detailed description of entropy generation minimization (EGM) analysis. In order to perform EGM analysis, we should proceed according to Ref. [28] and express the entropy generation rate N_s "as a function of the topology and physical characteristics of the system, namely, finite dimensions, shapes, materials, finite speeds, and finite-time intervals of operation." For reasons listed below, it will be unnecessary to perform EGM analysis for our current investigation and hence the computational results presented for entropy generation rates will be considered sufficient.

6.1 Topology and material properties

We investigate the flow in a channel of constant shape and dimensions. Minimizing the entropy generation rates with respect to the topological characteristics of the problem will thus be inappropriate in the current investigation. We also limit our investigation to fluids and materials of constant composition and hence, for the same reason, EGM analysis with respect to material properties will not be necessary.

6.2 Time

Our results suggest that the lowest entropy generation rates occur in steady state. An attempt to perform an EGM analysis to obtain the optimal required time is thus inappropriate.

6.3 Speeds

The finite suction/injection velocity may appear as the most

plausible flow characteristic on which to base an EGM analysis on. These speeds are measured in terms of the suction Reynolds number Re. However, Fig. 23 shows four regions in which the entropy generation rates alternate in magnitude for high and low Re values. For example, close to the injection wall, low entropy generation rates are recorded at higher Re values whereas the opposite behavior is observed close to the suction wall. These results thus show that is will not be possible to find an optimal Re value such that the entropy generation rates are minimized throughout the channel.

7. Conclusions

We have computationally investigated the transient pressure driven flow of a fluid in the presence of constant suction/injection at the walls and employed second law analysis to study the irreversibility properties within the flow field. The suction/injection shifts the regions of maximum velocity away from the centerline and leads to non-symmetry in the velocity and temperature gradients. Close to the left wall which is subjected to fluid injection, the fluid friction with magnetic field irreversibility strongly dominates over heat transfer irreversibility. This observation also obtains inside the main channel away from the right wall. Close to the right wall, which is subjected to fluid suction, the strength of the fluid parameters will determine which mode of irreversibility dominates over the other. It is thus possible to choose parameter values so that heat transfer irreversibility dominates in the vicinity of right wall region.

References

[1] J. Hartmann and F. Lazarus, Hg-Dynamics II, Theory of laminar flow of electrically conductive Liquids in a Homogeneous Magnetic Field, 15 (7) (1937).

[2] N. Riley, Magnetohydrodynamics free convection, *J. Fluid Mech*., 18 (1964) 577-586.

[3] A. J. Chamkha, Unsteady hydromagnetic natural convection in a fluid-saturated porous medium channel, *Adv. Filtration Separation Technol*., 10 (1996) 369-375.

[4] J. C. R. Hunt, Magnetohydrodynamic flow in a rectangular duct, *J. Fluid Mech.*, 21 (1965) 577-590.

[5] L. Buhler, Laminar buoyant magnetohydrodynamic flow in a vertical rectangular ducts, *Phys. Fluids*, 10 (1998) 223-236.

[6] J. A. Shercliff, Steady motion of conducting fluids in pipes under transverse magnetic fields, *Proc. Cambridge Philos. Soc*., 49 (1953) 136-144.

[7] T. Alboussiere, J. P. Garandet and R. Moreau, Buoyancy-driven convection with a uniform magnetic field, Part 1: Asymptotic analysis, *J. Fluid Mech.* (253) (1983) 545-563.

[8] O. D. Makinde and A. Aziz, MHD mixed convection from a vertical plate embedded in a porous medium with a convective boundary condition, *International Journal of Thermal Science*, 49 (2010) 1813-1820.

[9] O. D. Makinde and O. O. Onyejekwe, A numerical study of MHD generalized Couette flow and heat transfer with variable viscosity and electrical conductivity, *Journal of Magnetism and Magnetic Materials*, 323 (2011) 2757-2763.

[10] A. Bejan, A study of entropy generation in fundamental convective heat transfer, *J. Heat Transfer*, 101 (1979) 718-725.

[11] A. Bejan, *Entropy generation minimization*, CRC Press, New York (1996).

[12] O. D. Makinde, Irreversibility analysis of variable viscosity channel flow with convective cooling at the walls, *Canadian Journal of Physics*, 86 (2) (2008) 383-389.

[13] O. D. Makinde, Entropy-generation analysis for variable-viscosity channel flow with non-uniform wall temperature, *Applied Energy*, 85 (2008) 384-393.

[14] O. D. Makinde, Thermodynamic second law analysis for a gravity driven variable viscosity liquid film along an inclined heated plate with convective cooling, *Journal of Mechanical Science and Technology*, 24 (4) (2010) 899-908.

[15] Mehdi Kiyasatfar et al., Thermal behavior and entropy generation rate analysis of a viscous flow in MHD micropumps, *Journal of Mechanical Science and Technology*, 26 (6) (2012) 1949-1955.

[16] T. B. Chang and F. J. Wang, An analytical investigation into the Nusselt number and entropy generation rate of film condensation on a horizontal plate, *Journal of Mechanical Science and Technology*, 22 (2008) 2134-2141.

[17] H. Kucuk, Numerical analysis of entropy generation in concentric curved annular ducts, *Journal of Mechanical Science and Technology*, 24 (9) (2010) 1927-1937.

[18] A. Z. Sahin, A second law comparison for optimum shape of duct subjected to constant wall temperature and laminar flow, *Heat Mass Transfer*, 33 (1998) 425-430.

[19] S. H. Tasnim and S. Mahmud, Entropy generation in a vertical concentric channel with temperature dependent viscosity, *Int. Comm. Heat Mass Transfer*, 29 (7) (2002) 907-918.

[20] S. Mahmud and R. A. Fraser, Thermodynamic analysis of flow and heat transfer inside channel with two parallel plates, *Energy*, 2 (2002) 140-146.

[21] V. S. Arpaci, A. Selamet and S. H. Kao, *Introduction to heat transfer*, Prentice-Hall, New York (2000).

[22] O. D. Makinde and O. Anwar Beg, On inherent irreversibility in a reactive hydromagnetic channel flow, *Journal of Thermal Science*, 19 (1) (2010) 72-79.

[23] L. C. Woods, *Thermodynamics of fluid systems*, Oxford University Press, Oxford (1975).

[24] T. Chinyoka, Computational dynamics of a thermally decomposable viscoelastic lubricant under shear, *Transactions of ASME, J. Fluids Engineering*, 130 (12) (2008) 121201(7pages).

[25] T. Chinyoka, Poiseuille flow of reactive Phan-Thien-Tanner liquids in 1D channel flow, *Transactions of ASME, J. Heat Transfer*, 132 (11) (2010) 111701(7pages).

[26] T. Chinyoka and O. D. Makinde, Computational dynamics of unsteady flow of a variable viscosity reactive fluid in a porous pipe, *Mechanics Research Communications*, 37 (2010) 347-353.

[27] T. Chinyoka, Suction-injection control of shear banding in

non-isothermal and exothermic channel flow of Johnson-Segalman liquids, *Transactions of ASME, J. Fluids Engineering*, 133 (7) (2011) 071205(12pages).

[28] A. Bejan, Fundamentals of exergy analysis, entropy generation minimization, and the generation of flow architecture, *Int. J. Energy Res*., 26 (2002) 545-565.

Tirivanhu Chinyoka obtained a BSc (Hons) and MSc. degrees in Mathematics from the University of Zimbabwe and a Ph.D. in Applied Mathematics from Virginia Tech (USA). Dr Chinyoka's research interests are in computational analysis of temperature dependent flow of Newtonian and non-Newtonian fluids. He currently lectures at the University of Cape Town and is also currently the Vice President of the South African Association for Theoretical and Applied Mechanics (SAAM).

Oluwole Daniel Makinde is a Senior Professor & Director of Postgraduate Studies and Director of Institute for Advance Research in Mathematical Modelling and Computations, Cape-Peninsula Univ. of Technology, Bellville, RSA. He obtained his Ph.D. in Applied Mathematics from University of Bristol, UK. He is the winner of the prestigious 2011 African Union Kwame Nkrumah Continental Scientific Award from African Heads of States for his outstanding contribution to Basic Sciences, Technology and Innovation, Winner of South African National Science & Technology Forum and National Research Foundation 2009-2010 TW Kambule Senior Black Researcher Award for his outstanding contribution to Science, Engineering, Technology and Innovation. He has also won several distinctions, scholarships, fellowships and prizes and awards. Professor Makinde is the Secretary General of African Mathematical Union, Advisory board member of Pan African Centre of Mathematics (PACM) based in Dar es Salaam, Tanzania, Scientific committee member of Centre for Applied Research in Mathematical Sciences (CARMS) at Strathmore University in Kenya and an associate member of National Institute of Theoretical Physics (NITheP) in South Africa. He attended several conferences, seminars, workshops, etc., and presented keynote research papers. He has over 30 years of teaching and research experience, taught several courses and published 4 books and monographs and over 200 research papers. He has been editor/reviewer for numerous international journals. He supervised several Ph.D. and Master students in the field of Applied Mathematical Modelling and Computations. He has been awarded with several research grants. He has been External Examiner examining Ph.D. theses to several Universities and External Assessor for many Universities assessing the research papers for the suitability of promotion of several academic staff.